

<https://doi.org/10.1038/s42003-024-06735-z>

miR-29 is an important driver of aging-related phenotypes



Vijay Swahari^{1,12}, Ayumi Nakamura^{1,2,12}, Emilie Hollville^{1,3,12}, Yu-Han Hung⁴, Matt Kanke⁴, C. Lisa Kurtz⁵, Xurde M. Caravia⁶, David Roiz-Valle⁶, Shenghui He^{5,7}, Janakiraman Krishnamurthy^{5,7}, Sahil Kapoor¹, Varun Prasad¹, Cornelius Flowers¹, Matt Beck¹, Jeanette Baran-Gale^{5,8}, Norman Sharpless^{5,7}, Carlos López-Otín^{6,9,10}, Praveen Sethupathy⁴ & Mohanish Deshmukh^{1,2,11}

Aging is a consequence of complex molecular changes, but whether a single microRNA (miRNA) can drive aging remains unclear. A miRNA known to be upregulated during both normal and premature aging is miR-29. We find miR-29 to also be among the top miRNAs predicted to drive aging-related gene expression changes. We show that partial loss of miR-29 extends the lifespan of *Zmpste24*^{-/-} mice, an established model of progeria, indicating that miR-29 is functionally important in this accelerated aging model. To examine whether miR-29 alone is sufficient to promote aging-related phenotypes, we generated mice in which miR-29 can be conditionally overexpressed (miR-29TG). miR-29 overexpression is sufficient to drive many aging-related phenotypes and led to early lethality. Transcriptomic analysis of both young miR-29TG and old WT mice reveals shared downregulation of genes associated with extracellular matrix organization and fatty acid metabolism, and shared upregulation of genes in pathways linked to inflammation. These results highlight the functional importance of miR-29 in controlling a gene expression program that drives aging-related phenotypes.

MicroRNAs (miRNAs) are important regulators of a wide range of physiological functions¹ and have emerged as candidate therapeutic targets for a number of diseases^{2,3}. Many miRNAs, such as miR-29 family members, are widely expressed across different tissues and developmental stages. The miR-29 family has been closely studied for years by our team and others, and has been implicated in the regulation of many biological processes including but not limited to apoptosis⁴, metabolism⁵, lipogenesis^{6,7}, energy balance^{8,9}, brain maturation^{10,11}, immunity^{12,13}, tumor suppression and metastasis¹⁴, and fibrosis¹⁵.

As many of these processes are linked to aging, it is perhaps not surprising that the miR-29 family is also known to be induced during normal aging^{16–19}. The miR-29 family is comprised of miR-29a, miR-29b, and miR-29c miRNAs that are expressed from two genomic loci: *miR-29a/b-1* (located on chromosome 7 for *H. sapiens*, chromosome 3 for *M. mulatta* and chromosome 6 for *M. musculus*) and *miR-29b-2/c* (located

on chromosome 1 for *H. sapiens*, *M. mulatta* and *M. musculus*)²⁰. The miR-29 sequence is broadly evolutionarily conserved (though known by a different name in some non-mammalian species such as miR-83 in *C. elegans*²¹) and the seed sequence, which plays an essential role in the targeting of mRNAs, is identical across mammals including primates and rodents²⁰. A recent study found that the expression of the miR-29 family positively correlates with aging in solid organs, extracellular vesicles, and plasma in mice¹⁹. This study also found that in mice rejuvenated by heterochronic parabiosis, one member of the miR-29 family (miR-29c-3p) was the most prominent miRNA restored to similar levels found in young liver¹⁹. miR-29 was also reported to be elevated in two mouse models of premature aging^{22–24} and, interestingly, is also one of only two miRNAs that are reduced in the Ames Dwarf mouse model in which the onset of aging is delayed²⁵. Despite this strong correlation of miR-29 levels with normal, premature, and delayed aging, whether

¹Neuroscience Center; University of North Carolina, Chapel Hill, NC, USA. ²Neurobiology Curriculum; University of North Carolina, Chapel Hill, NC, USA. ³Institute of Medical Sciences, University of Aberdeen, Aberdeen, UK. ⁴Department of Biomedical Sciences; College of Veterinary Medicine, Cornell University, Ithaca, NY, USA. ⁵Department of Genetics; University of North Carolina, Chapel Hill, NC, USA. ⁶Departamento de Bioquímica y Biología Molecular, Instituto Universitario de Oncología (IUOPA), Universidad de Oviedo, Oviedo, Spain. ⁷The Lineberger Comprehensive Cancer Center; University of North Carolina, Chapel Hill, NC, USA. ⁸Bioinformatics and Computational Biology Curriculum; University of North Carolina, Chapel Hill, NC, USA. ⁹Centro de Investigación Biomédica en Red de Cáncer (CIBERONC), Madrid, Spain. ¹⁰Instituto de Investigación Sanitaria del Principado de Asturias (ISPA), Oviedo, Spain. ¹¹Department of Cell Biology and Physiology, University of North Carolina, Chapel Hill, NC, USA. ¹²These authors contributed equally: Vijay Swahari, Ayumi Nakamura, Emilie Hollville.

✉ e-mail: pr46@cornell.edu; mohanish@med.unc.edu

upregulation of miR-29 is sufficient to drive the aging phenotype *in vivo* has not been investigated.

Here, we confirmed the induction of miR-29 in multiple aging contexts. As a complementary approach, we also found that the genes downregulated during aging in mice are enriched for predicted targets of miR-29. To examine the functional importance of miR-29 in aging, we generated mouse models in which miR-29 levels could be reduced or elevated. Reduction of miR-29 increased lifespan in a progeria model whereas inducing miR-29 alone was sufficient to accelerate aging in mice. Lastly, we conducted transcriptomic analysis to highlight miR-29-regulated gene expression changes that may drive aging.

Results

miR-29 levels are increased in multiple tissues and animal models of aging

We first sought to characterize the elevation of miR-29 in different models of aging. We examined the levels of the miR-29 family in Rhesus macaque liver and found miR-29 levels to increase with age (Fig. 1a and Supplementary Fig. 1a). We next measured miR-29 family members in the *Lmna*^{G609G} mouse model of progeria²⁶ and found that while all three miRNAs are trending upward, only miR-29b-3p is significantly elevated in this model of accelerated aging (Supplementary Fig. 1b). Based on these results, and because miR-29b is expressed from both genomic loci, we focused on miR-29b-3p for our subsequent studies in mice. We showed that miR-29b levels are significantly increased with age in multiple tissues in mice (Fig. 1b).

miR-29 target genes are enriched within genes downregulated in aging

To determine the functional capacity of miR-29 to drive molecular changes during aging, we conducted an unbiased query of the genes that are differentially expressed in the liver during normal aging in mice (Fig. 1c). We found that the genes significantly downregulated ($n = 352$, FDR < 0.1) in 2-year-old mice relative to 2-month-old mice are significantly enriched for predicted targets of miR-29 (Fig. 1d). Expectedly, the significantly upregulated genes ($n = 448$, FDR < 0.1) do not harbor any enrichment for miR-29 targets (Supplementary Fig. 2a). We repeated this analysis after stratification by sex and found that miR-29 is the only miRNA with significant enrichment of predicted targets among downregulated genes in both aged males and females (Supplementary Fig. 2c–j). An unbiased pathway analysis of the downregulated genes in aged mice revealed enrichment in collagen and extracellular matrix components, which are well known targets of miR-29²⁷ (Fig. 1e), while the upregulated genes are enriched in pathways associated with sphingolipid metabolism and neutrophil-mediated immune response (Supplementary Fig. 2b). These results strongly suggest that the gene expression changes during aging could be a consequence of elevated levels and activity of miR-29.

miR-29 reduction extends lifespan in a progeria model

We next examined whether reducing miR-29 levels could extend the survival of the *Zmpste24*^{-/-} mice, an established model of progeria^{28,29}. The *Zmpste24*^{-/-} mouse model is particularly relevant because all three miR-29 family members have previously been shown to be aberrantly elevated in *Zmpste24*^{-/-} mice²². Unfortunately, the complete deletion of miR-29 (deletion of both *miR-29a/b-1* and *miR-29b-2/c* loci) results in early lethality^{10,30}, precluding us from examining the consequences of a total loss of miR-29 in the context of aging. We, therefore, crossed the *Zmpste24*^{-/-} mice with mice deficient for only the *miR-29a/b-1* locus to examine the consequence of partial reduction of miR-29 on the survival of the *Zmpste24*^{-/-} mice. We used mice deleted for the *miR-29a/b-1* locus because it has been reported as the dominant source of miR-29b³¹. Strikingly, we found that the *miR-29a/b-1*^{+/-} *Zmpste24*^{-/-} mice exhibit a significant lifespan extension compared with *miR-29a/b-1*^{+/+} *Zmpste24*^{-/-} mice (median survival 141 versus 118 days, $p = 0.005$), indicating that miR-29 is important for driving premature aging in this progeria model (Fig. 1f). Also, consistent with the observed extension of lifespan, the elevation of miR-29 levels seen in the *Zmpste24*^{-/-} mice was

markedly reduced, even with a partial deletion of the *miR-29a/b-1* locus, at three months when the lifespan differences emerge (Fig. 1g).

Increasing miR-29 alone is sufficient to induce an aging phenotype

Next, we sought to determine whether increased expression of miR-29 is sufficient to drive aging-related phenotypes *in vivo*. To examine this, we generated transgenic mice that overexpress miR-29b (henceforth referred to as miR-29) ubiquitously under a tetracycline-inducible promoter (miR-29TG) (Fig. 2a). Strikingly, by 2 months, overexpression of miR-29 led to an overt aging-like phenotype (Fig. 2b). The levels of miR-29b-3p overexpression (2–4 fold) obtained with doxycycline administration in these miR-29TG mice (Fig. 2c) are comparable to the fold increase in miR-29b-3p seen with age in WT mice (Fig. 1b). The miR-29TG mice exhibited growth retardation and premature death, with all mice dying by 80 days (Fig. 2d, e).

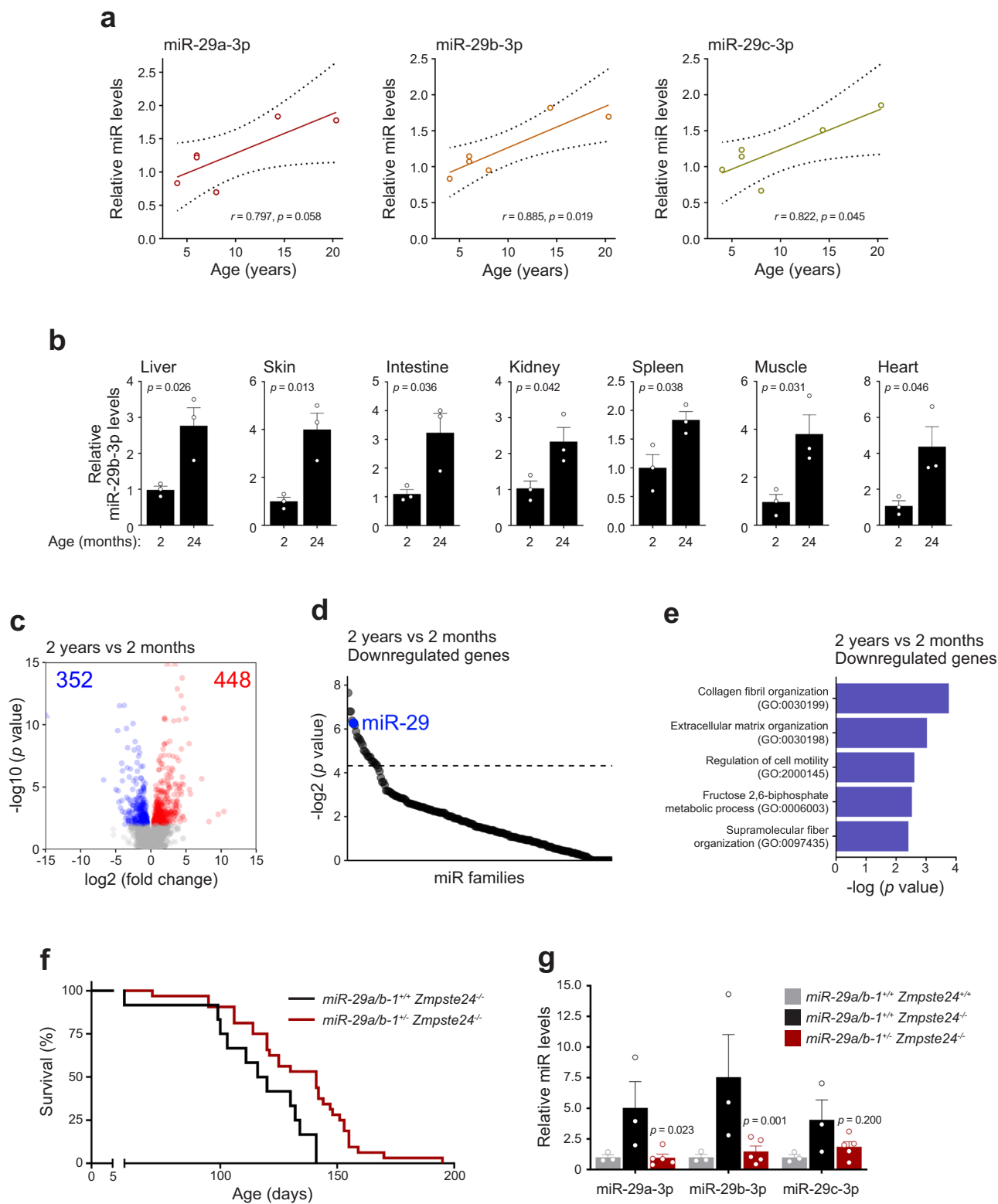
Starting at approximately one month of age, miR-29TG mice began to display premature graying of hair as well as extensive kyphosis that was confirmed using Computed Tomography (CT) imaging analysis (Fig. 3a, b). The miR-29TG mice also exhibited severe lipodystrophy characterized by little or absent inguinal fat pads at 2 months (Fig. 3c). Further, these mice showed reduced skin thickness and increased collagen deposits in all layers of the dermis and epidermis (Fig. 3d, e). A prominent feature of both normal aging and progeria is the development of osteoporosis. We conducted bone densitometry studies using micro-CT analysis and found that miR-29TG mice indeed have signs of severe osteoporosis as characterized by reduced cortical and trabecular bone volume, reduced cortical bone mineral and total density, and reduced trabecular bone thickness (Fig. 3f–i and Supplementary Fig. 3a–c). Similar reductions in bone volume have been observed in the *Lmna*^{G609G} mouse model of progeria²⁶. In addition, thymus weight and cellularity were reduced in miR-29TG mice, and the normal sequence of thymocyte maturation was disrupted (Supplementary Fig. 4a–d). Interestingly, the frequency of phenotypic hematopoietic stem cells (HSCs) in the bone marrow and spleen was significantly reduced in the miR-29TG mice (Supplementary Fig. 4e, f). Thus, miR-29 overexpression results in many phenotypes that are known to be associated with aging³².

Increased cellular senescence is often associated with aging, and one of the most well-recognized senescence marker is positive staining with senescence-associated beta-galactosidase (SA-β-gal)³³. To determine whether miR-29TG mice exhibit increased senescence, we conducted the SA-β-gal assay on kidneys isolated from young (2 months) miR-29TG, their WT littermates, as well as old (2 years) WT mice. In contrast to young WT controls, the miR-29TG kidneys showed strongly positive SA-β-gal staining similar to what was observed in old WT kidneys (Fig. 3j). Taken together, these findings show that overexpression of miR-29 is sufficient to induce multiple features of an aging-like phenotype in mice.

miR-29-driven transcriptome changes associated with aging

To define the pathways that are altered in the miR-29TG mice, we conducted RNA-seq analysis of liver tissue from young (2 months) WT and miR-29TG mice. Principal component analysis showed that the mice stratify clearly by genotype status, irrespective of sex (Supplementary Fig. 5a). We found a large number of genes to be differentially expressed between miR-29TG mice and WT mice (1928 genes downregulated and 2076 genes upregulated, FDR < 0.1) (Supplementary Fig. 5b). The downregulated genes are highly enriched in fatty acid metabolism (Fig. 4a), while the upregulated genes are highly enriched in pathways related to inflammation, including neutrophil activation (Fig. 4b).

We next sought to identify the shared genes that are significantly altered in both young miR-29TG and old WT mice relative to young WT mice, as these genes may directly contribute to the aging phenotype. We detected 163 significantly downregulated (FDR < 0.1) and 234 significantly upregulated (FDR < 0.1) genes shared by young miR-29TG and old WT when compared to young WT mice (Fig. 4c, d). Notably, we found that the shared set of up- and downregulated genes are significantly over-represented in many of the same pathways as the old WT



mice (Fig. 4e, f and Supplementary Data 1, 2). As anticipated, several of the shared downregulated genes are predicted targets of miR-29 (Supplementary Data 3). Among the shared downregulated genes are collagen type 1 alpha 1 chain (*Col1a1*) and collagen type 3 alpha 1 chain (*Col3a1*) (Fig. 4g, h), both of which are targets of miR-29³⁴ and have been previously associated with aging³⁵. Another shared downregulated gene is cAMP signaling calcium/calmodulin-dependent protein kinase IV

(*Camk4*) (Fig. 4i and Supplementary Data 1), a highly conserved predicted target of miR-29, which was previously found to be the most robustly downregulated gene in brains of aged mice, monkeys, and humans³⁶. Other predicted miR-29 target genes in this shared downregulated data set also include *Cd276* (B7-H3) which is known to suppress senescence³⁷ and *Jazf1* a transcription factor that regulates glucose and lipid metabolism³⁸.

Fig. 1 | miR-29 is a candidate driver of gene expression changes in aged mice.
a Correlation analysis of the change in levels of miR-29 family members with age in the liver of male Rhesus macaque. Pearson correlation r is represented.
b Quantitative PCR analysis for mature miR-29b-3p in multiple tissues from 2-month and 24-month-old mice ($n = 3$). p values were calculated using an unpaired t -test. Data shown are mean \pm s.e.m. **c** Volcano plot showing significantly upregulated (red) and downregulated (blue) genes in liver from old (2 years) mice ($n = 5$; 3 males, 2 females) compared to liver from young (2 months) mice ($n = 5$; 3 males, 2 females). Filtering criteria: $p < 0.05$, adjusted $p < 0.2$ (Wald test; DESeq2). **d** miRHub analysis of the downregulated genes in 2-year-old mouse liver compared to 2-month-old mouse liver. Predicted target sites of the miR-29 family (blue) are significantly enriched in the set of downregulated genes. Dashed line corresponds to

$p = 0.05$. **e** Pathway enrichment analysis of the genes that are significantly downregulated in old compared to young mouse liver. The analysis was performed based on Gene Ontology (GO) Biological Process 2021. The top 5 processes are represented. **f** Kaplan–Meier survival curve of *miR-29a/b-1^{+/+} Zmpste24^{-/-}* and *miR-29a/b-1^{-/-} Zmpste24^{-/-}* mice ($p = 0.005$, Log-rank/Mantel-Cox test). The median survival is 118.0 days for *miR-29a/b-1^{+/+} Zmpste24^{-/-}* and 141.0 days for *miR-29a/b-1^{-/-} Zmpste24^{-/-}*. **g** Quantitative PCR analysis of miR-29 family members in the heart of *miR-29a/b-1^{+/+} Zmpste24^{+/+}* ($n = 3$), *miR-29a/b-1^{+/+} Zmpste24^{-/-}* ($n = 3$) and *miR-29a/b-1^{-/-} Zmpste24^{-/-}* ($n = 5$) mice (males, 3 months old). p values were calculated using two-way ANOVA, against *miR-29a/b-1^{+/+} Zmpste24^{-/-}*. Data shown are mean \pm s.e.m.

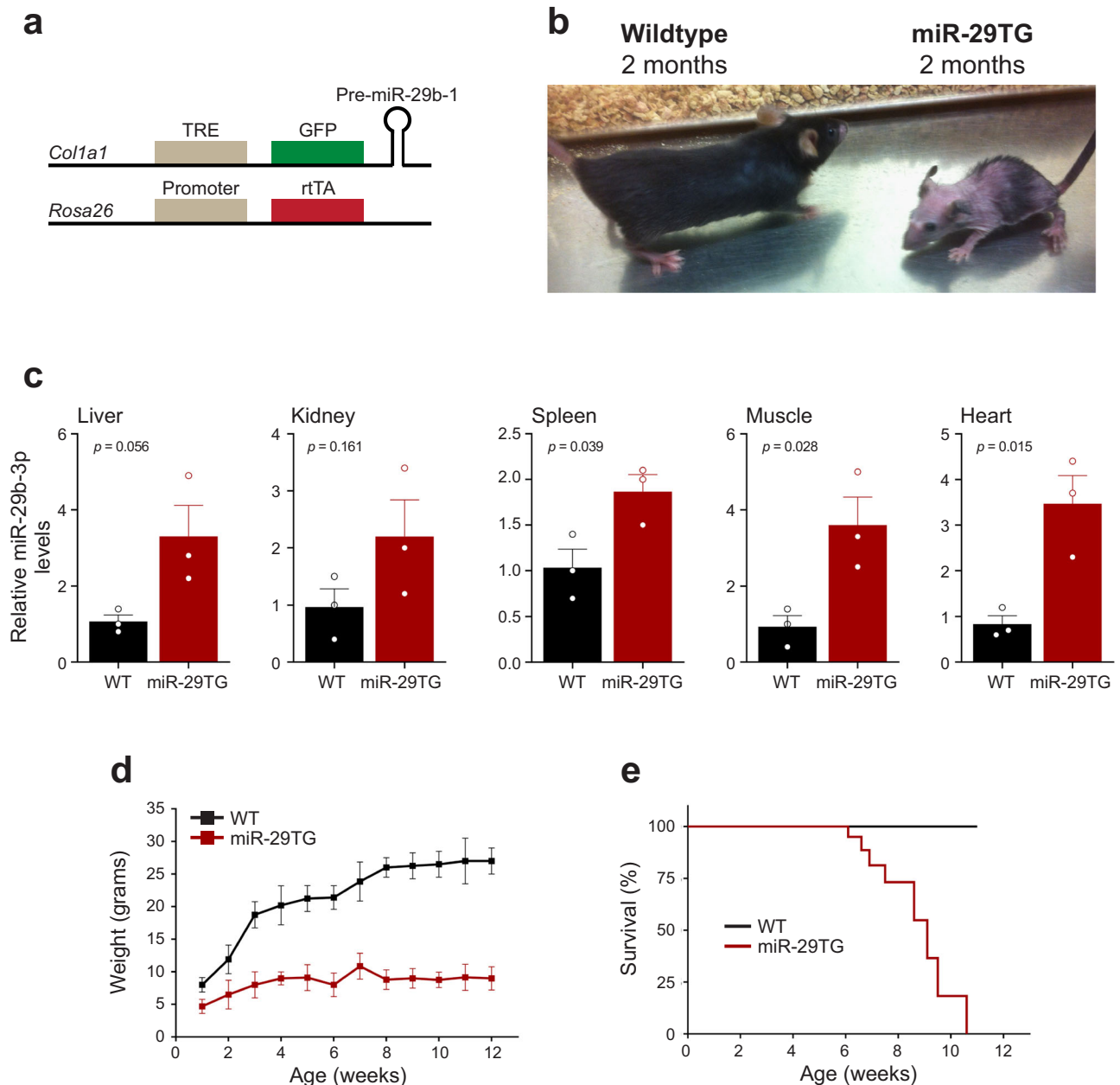


Fig. 2 | Overexpression of miR-29 results in growth retardation and premature death in mice. **a** Constructs used to generate the miR-29 transgenic (miR-29TG) mice. miR-29b-1 and GFP are expressed under the control of tetracycline response element (TRE). In the presence of doxycycline, the tetracycline response transactivator (rtTA) enables TRE-driven expression of miR-29b-1 and GFP. **b** Wildtype (left) and miR-29TG (right) mice at 2 months; miR-29 was induced with doxycycline

starting at postnatal day 1. **c** Quantitative PCR analysis of mature miR-29b-3p levels in the indicated tissues of miR-29TG mice as compared to WT mice (2 months) ($n = 3$). p values were calculated using an unpaired t -test. **d** Weights ($n = 3$) and **e** Kaplan–Meier survival curve of WT and miR-29TG mice ($n = 12$ for each genotype). The median survival of miR-29TG mice is 91 days. Data shown are mean \pm s.e.m. in **c** and **d**.

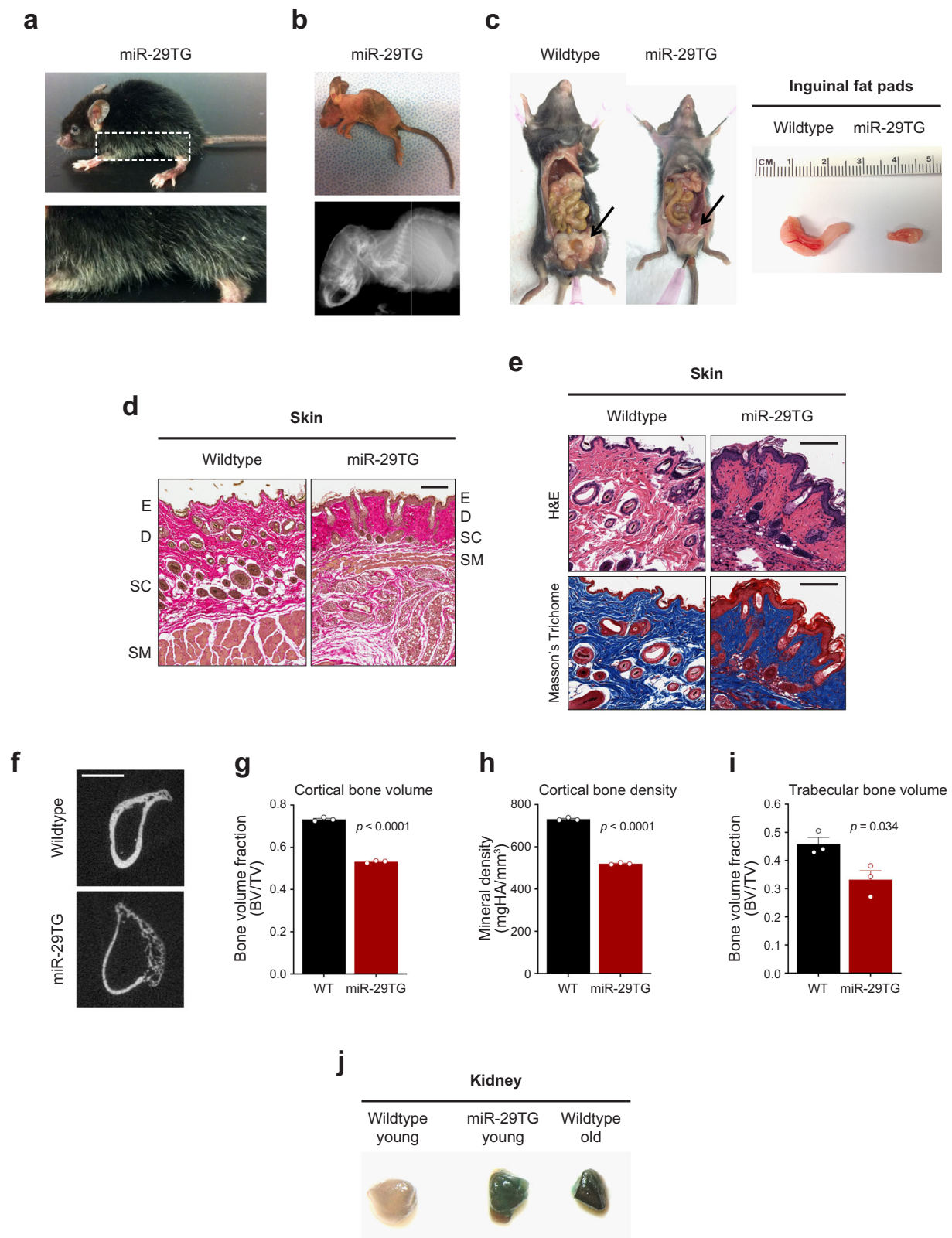


Fig. 3 | miR-29TG mice exhibit signs of premature aging. **a** miR-29TG mice develop hair graying and **b** kyphosis (top, photograph; bottom, CT scan) by 2 months. **c** Left: lipodystrophy observed in 2-month-old miR-29TG mice (arrows). Right: inguinal fat pads of wildtype and miR-29TG mice. **d** Skin of wildtype and miR-29TG mice (2 months) stained with elastin. Epidermis (E), dermis (D), subcutis (SC), and subcutaneous muscle (SM) layers are highlighted. Scale bar: 150 μ m. **e** Increased collagen deposition (H&E, Masson's Trichrome staining) in the skin of miR-29TG mice. Scale bar: 150 μ m. **f** MicroCT scan images of the femur of wildtype

and miR-29TG mice (2 months). Scale bar: 1 mm. **g–i** Femoral bone volume and bone mineral density were quantified (wildtype, $n = 3$; miR-29TG, $n = 3$). **g** Cortical and **i**, trabecular bone volume (BV) is shown as a fraction relative to total bone volume (TV). Data shown are mean \pm s.e.m., p values were calculated using an unpaired t -test. **j** Senescence-associated β -gal staining of the kidneys of young (2 months) wildtype, young (2-month-old) miR-29TG, and old (2-year-old) wildtype animals.

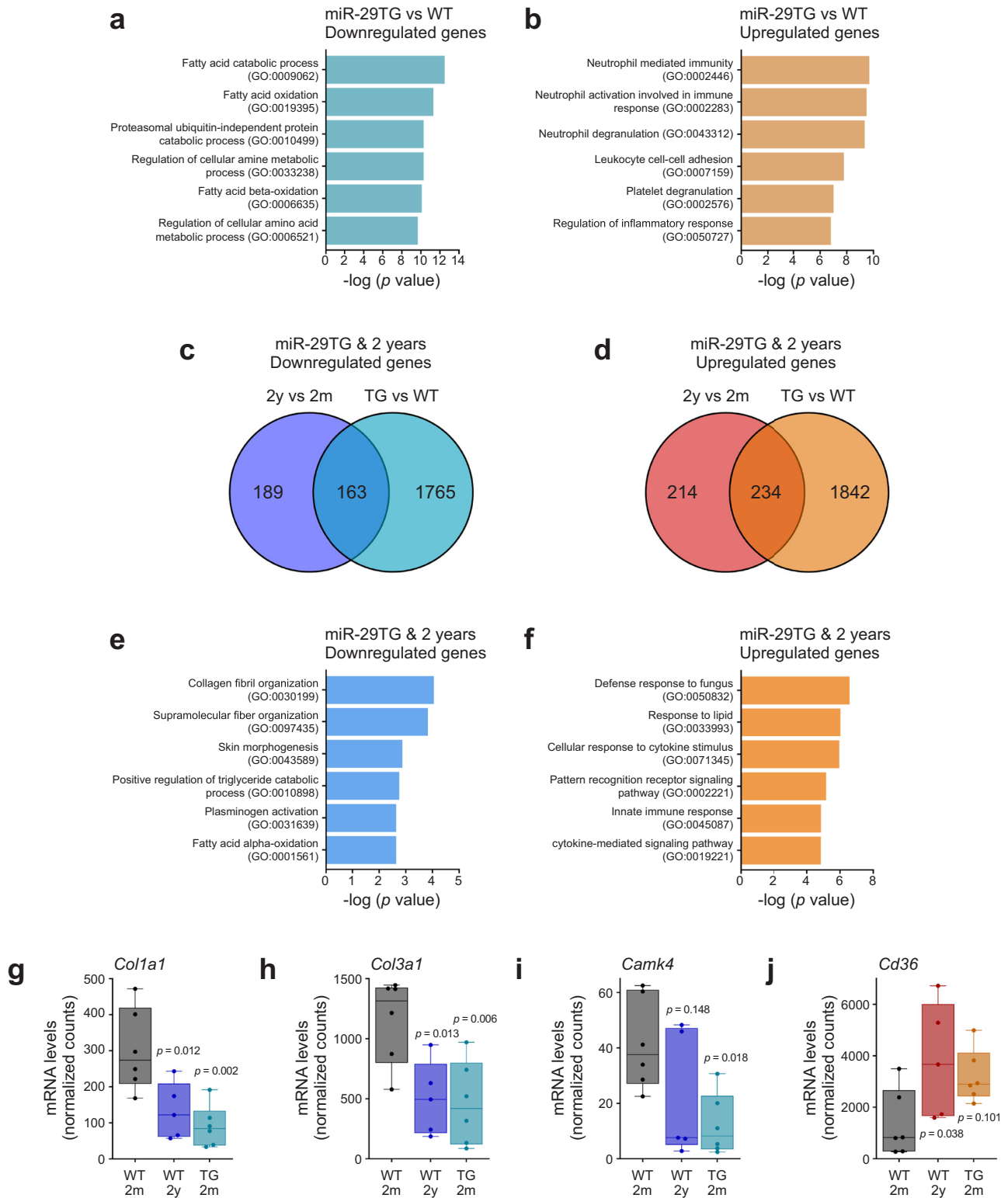


Fig. 4 | The liver of miR-29TG and 2 year-old wildtype mice share changes in key aging-related genes and pathways. a, b Pathway enrichment analysis of the genes that are significantly **a** downregulated and **b** upregulated in the liver of 2-month-old miR-29TG mice ($n = 6$; 5 males, 1 female) compared to 2-month-old wildtype mice ($n = 6$; 4 males, 2 females). The analysis was performed based on Gene Ontology (GO) Biological Process 2021. The top 6 processes are represented. **c–j** Comparison of the genes differentially expressed in the liver of 2-year-old wildtype mice and 2-month-old miR-29TG mice. **c, d** Number of genes **c**, downregulated and **d**, upregulated in common between the liver of 2-month-old (2 m) miR-29TG and the liver of 2-year-old (2 y) wildtype mice relative to 2-month-old (2 m) wildtype mice. **e, f** Pathway enrichment analysis of shared **e** downregulated genes and

f upregulated genes between the liver of 2-month-old miR-29TG and 2-year-old wildtype mice. Analysis was performed based on Gene Ontology (GO) Biological Process 2021. The top 6 processes are represented. **g–j**, Expression of **g** *Col1a1*, **h** *Col3a1*, **i** *Camk4* and **j** *Cd36* mRNA in the liver of 2-month-old wildtype ($n = 6$; 4 males, 2 females), 2-year-old wildtype ($n = 5$; 3 males, 2 females) and 2-month-old miR-29TG mice ($n = 6$; 5 males, 1 female). The median, minimum and maximum are represented. The adjusted p values were calculated using unpaired one-way ANOVA followed by pairwise comparisons with Dunnett correction, comparing all samples to 2-month-old wildtype.

A shared upregulated gene is *Cd36*, a membrane glycoprotein involved in fatty acid transport (Fig. 4j, Supplementary Data 2). Previous studies have found *Cd36* to not only be upregulated in the hearts of aged mice but also to contribute to age-induced cardiomyopathy³⁹. Interestingly, *Cd36* is also upregulated in response to senescence stimuli and is required for the senescence-associated secretory phenotype (SASP)⁴⁰. Further, ectopic expression of *Cd36* alone is sufficient to induce many components of SASP⁴⁰ as well as induce senescence in young proliferating cells⁴¹. Interestingly, miR-29 has also been reported to induce cellular senescence *via* other pathways⁴². Thus, our study not only identifies genes that were previously known to be functionally associated with aging, but also reveals other genes (Supplementary Data 1, 2) that could be important to drive aging-related phenotypes mediated by miR-29.

Discussion

Taken together, our results highlight miR-29 as a tissue marker of aging in primates and mice, and an important molecular regulator of aging-related phenotypes in mice. The concept that a single miRNA could regulate as complex a process as aging seems provocative, but individual miRNAs are well-recognized to have the ability to regulate very diverse cellular pathways⁴³. While elevated levels of miR-29 have been previously reported to be associated with aging^{16–18,22,23,44}, our study demonstrates that miR-29 is sufficient to accelerate aging and drive aging-related phenotypes *in vivo*. Importantly, we also found the reduction of miR-29 to extend lifespan in a progeria model.

Our knowledge about the pathways that are functionally important for regulating aging has come mostly from genetic studies in invertebrates and from mouse models of progeria. In mouse models of progeria, the mutations that cause aging are associated with either maintenance of nuclear architecture (e.g., Hutchinson-Gilford Progeria Syndrome) or genomic integrity (e.g., Werner's syndrome, Cockayne syndrome)⁴⁵. While many of the phenotypes seen in these progeroid models are also observed during normal aging, it is unclear whether the same genes drive the aging phenotype in both models. Our results suggest that miR-29 could be a candidate that regulates both pathological and physiological aging.

We propose that the pathways that are shared in multiple models of aging are likely to be more important for driving the aging phenotype. Our analysis of the genes shared between the miR-29TG mice and old mice highlights the downregulation of collagen synthesis (e.g. *Coll1a1*, *Col3a1*), kinase signaling (*Camk4*), and the upregulation of *Cd36* as potential drivers of the aging phenotypes. One mechanism by which *Camk4* could regulate aging is *via* its modulation of autophagy⁴⁶, the reduction of which is a hallmark of aging³². This is consistent with the finding that the ortholog of miR-29 in *Caenorhabditis elegans*, miR-83, is elevated during aging and has been shown to reduce lifespan *via* inhibition of autophagy^{21,47}. Pathway analysis also identified an upregulation of immune response in these models, a finding consistent with the well-recognized increase in inflammation in age-related disease and aging^{32,48,49}. Interestingly, we found three components (C6, C8A, and C8B) of the complement system's Membrane Attack Complex (MAC) among the shared downregulated genes. Few studies have examined how the complement system changes with aging⁵⁰. Our finding that multiple components of MAC are downregulated with aging suggests that this could be functionally linked with aging.

The upstream mechanisms by which miR-29 is elevated with age in mammals are not well defined. Recent work shows that *Foxa2*, a known transcriptional activator of miR-29⁵¹, exhibits increased chromatin occupancy in liver tissue of aged mice as well as of *Zmpste24*^{-/-} mice⁵². It remains unknown whether *Foxa2* is the main driver of miR-29 during aging or whether other factors are involved.

It is also unclear which tissues or cell types within a particular tissue are most relevant for the miR-29-mediated aging phenotype. For example, an intriguing aspect about miR-29 is that its biological activity appears to be context-dependent. While increases in miR-29 levels with age are observed in multiple tissues, the pattern of its induction appears tissue-specific. In the brain, miR-29 levels increase sharply during postnatal maturation

(0–2 months) such that miR-29 levels are high even in the brains of young mice^{10,11}. Further, miR-29 has an essential function in brain maturation^{10,11}, and brain-specific deletion of miR-29 results in early lethality¹⁰. Marked increases in miR-29 levels during the postnatal maturation period are also observed in the heart and skeletal muscle, where miR-29 is also functionally important^{30,53,54}. Thus, the upregulation of miR-29 in the brain, heart and skeletal muscle is beneficial, and not detrimental, for homeostasis. Indeed, miR-29 is recognized to have therapeutic potential in the context of neurodegenerative and cardiovascular diseases^{53,55–58}. The expression of individual miRNAs can have distinct functional outcomes in mitotic *versus* postmitotic cells or even different cell types within these groups, depending on the repertoire of expression of its target genes. Higher-resolution single-cell studies during aging as well as future experiments focusing on elevating miR-29 expression in specific tissues or cell types will help identify the specific context in which elevated miR-29 drives the aging-related phenotypes.

Methods

Animals used in this study

Rhesus macaque (*M. mulatta*) liver samples were provided by the Havel lab at University of California-Davis. Tissues were collected from adult male monkeys (age range 4 – 20.3 years), which were maintained at the California National Primate Research Center and provided a standard commercial nonhuman primate diet (5047; LabDiet, St. Louis, MO). All animal procedures were performed with the approval and authorization of the Institutional Animal Care and Use Committee (IACUC).

The *Lmna*^{G609G} knock-in and *Zmpste24*^{-/-} mice were generated by the López-Otín lab. The *Lmna*^{G609G} knock-in mice carry a point mutation in the *Lmna* gene (1827C > T) that does not change the coding sequence (G609G) but activates a cryptic splicing donor site resulting in the generation of a truncated form of prelamin A (progerin). This point mutation in mice is equivalent to the mutation carried in Hutchinson-Gilford progeria syndrome patients²⁶. The presence of the *Lmna*^{G609G} knock-in mutation was verified by PCR using 5'-AGCATGCAATAGGGTGGAAAGGA-3' (forward) and 5'-AAGGGCTGGGAGGACAGAG-3' (reverse) primers. The *Zmpste24*^{-/-} mice are deleted for the *Zmpste24* gene, as described previously²⁹. 5'-GCTGGCCTTGTGCTGGAAT-3' (forward, wildtype specific), 5'-CTTCCGAGCGGATCTCAAA-3' (forward, mutant specific), and 5'-GCTTCCTCCCTGAGCCAACC-3' (reverse) primers were used to determine the *Zmpste24* genotype of the mice. The *Lmna*^{G609G} and *Zmpste24*^{-/-} mice are both well-established models of progeria⁵⁹.

The *miR-29a/b-1*^{+/-} mice were also generated by the López-Otín lab as described³⁰, from two embryonic stem (ES) cell lines carrying targeted deletions in the *miR-29a/b-1* and *miR-29b-2/c* clusters obtained from Dr. Haydn M. Prosser⁶⁰. To generate the *miR-29a/b-1*^{+/-} *Zmpste24*^{-/-} mice, we bred the *miR-29a/b-1*^{+/-} with *Zmpste24*^{+/-} mice to obtain *miR-29a/b-1*^{+/-} *Zmpste24*^{+/-} parental mice. By intercrossing *miR-29a/b-1*^{+/-} *Zmpste24*^{+/-}, we obtained *miR-29a/b-1*^{+/-} *Zmpste24*^{-/-} and *miR-29a/b-1*^{+/-} *Zmpste24*^{+/-} at frequencies consistent with the expected Mendelian ratio. The *miR-29a/b-1* genotype was determined by PCR using 5'-CGTTATTGCTGACGTTG-GAG-3' (forward, wildtype specific), 5'-TGTAACACGACGGCCAGTG-3' (forward, mutant specific), 5'-ATTGGTTTGGCCCTTTATCC-3' (reverse) primers. For the survival studies, mice were checked weekly. All animal experiments were approved by the Committee on Animal Experimentation of Universidad de Oviedo.

We have complied with all relevant ethical regulations for animal use.

Generation of miR-29TG mice

Mouse embryonic stem cells overexpressing miR-29b used to generate the miR-29TG mice were obtained from Dr. Gregory Hannon (Cold Spring Harbor Laboratory). The parental ES cell line used to produce the miR-29-expressing clones was KH2 (C57BL/6 × 129/Sv). These cells are now commercially available at the NCI Mouse Repository (ES Cell Lines Catalog: M000108). The presence of the miR-29b transgene was confirmed by PCR with the following primers: 5'-CACCTGAAAACCTTTGCCCC-3'

(forward) and 5'-GCACCATTTGAAATCAGTGTTTC-3' (reverse). The presence of the rTA promoter was confirmed by PCR with the following primers: 5'-GGAGCGGGAGAAATGGATATG-3', 5'-GCGAAGAGTTTGTCTCAACC-3', and 5'-AAAGTCGCTCTGAGTTGTAT-3'. To induce the expression of miR-29, a mixture of doxycycline (2 mg/ml) and sucrose (50 mg/ml) was added to the drinking water of both wildtype and miR-29TG mice starting on postnatal day 1. Mice were maintained in a 12 h light, 12 h dark cycle. The miR-29TG mice have been backcrossed to C57BL/6 mice and are maintained in the C57BL/6 background. All animal handling and protocols were carried out as approved by the Animal Care and Use Committee of the University of North Carolina (UNC).

Histology

For immunohistochemistry experiments, mice were anesthetized using isoflurane and transcardially perfused with 4% paraformaldehyde. The mice were then decapitated, and the various tissues were post-fixed in 4% paraformaldehyde overnight. Paraffin-embedded sections were used for hematoxylin-eosin (H/E), elastin, and Trichrome stains. Hematoxylin-eosin (H&E) stains were done using an Autostainer XL (Leica Biosystems). Representative images are obtained from independent experiments, done in triplicate.

cDNA synthesis and RT-qPCR analysis

Mature microRNA expression was assayed using TaqMan MicroRNA Assays (Applied Biosystems, catalog #4427975). Briefly, RNA was extracted from various tissues using the Qiagen miRNeasy kit (catalog #217004) or Invitrogen Trizol protocol (catalog #15596026). RNA was reverse transcribed using TaqMan miRNA reverse transcription kit (Applied Biosystems, catalog #4366596) and specific RT primers or TaqMan Advanced cDNA synthesis kit (Applied Biosystems, catalog #A28007) with 2.5 mM of random primers added to the RT stage of the cDNA synthesis kit. cDNA was then amplified using a TaqMan Universal PCR Master Mix (Applied Biosystems, catalog #4304437). Relative quantification was carried out using the delta-delta Ct method. Sample variability was corrected by normalizing to levels of U6 RNA (for WT and miR-29TG samples), snoRNA202 (for WT and LmnaG609G samples) or rRNA 18S (for WT, miR-29a/b-1^{+/+}; Zmpste24^{-/-} and miR-29a/b-1^{+/+}; Zmpste24^{-/-} samples).

Computed tomography imaging

Computed tomography (CT) images were acquired using a custom-built Charybdis II scanner with a carbon nanotube field emission x-ray source. The source was operated at 50 kVp, with a 1.5 mA anode current and 50 msec exposure. 220 projections were acquired and reconstructed in COBRA (Exxim Computing Corporation, Pleasanton, CA). The image voxel size was 75.7 μ m isotropic. For analysis of osteoporosis, samples were secured in a vertical orientation and scanned with a Scanco μ CT40⁶¹ (Scanco Medical AG, Switzerland). Samples were scanned using the following parameters: 70 kVp, 114 μ A, 8 W, 250 projections/slice, integration time 250 msec, and 12 μ m voxel size. Standard midshaft and trabecular bone analyses were conducted using the Scanco Medical software. First, a region of interest was selected using the contouring tool. The cortical midshaft analysis consisted of 50 slices (600 μ m) measured to be midway between the ends of the bone. For the trabecular analysis, 50 slices (600 μ m) were taken approximately 200 μ m from the end of the bone to avoid the growth plate. Regions of interest were drawn to include only trabecular bone in the analysis.

Senescence-associated β -gal staining

Senescence-associated β -gal staining was performed with the Cellular Senescence Assay Kit according to the manufacturer's instructions (Millipore).

Flow cytometry analysis

Two-month-old WT and miR-29TG mice were euthanized and bone marrow, spleen, and thymus cells were harvested following the standard

procedure as previously described⁶². Specifically, single-cell suspension of bone marrow cells was prepared by flushing the femurs and tibias using 3 ml ice-cold staining medium (Ca²⁺- and Mg²⁺-free Hank's balanced salt solution, HBSS (Gibco) supplemented with 10 mM EDTA (Corning) and 2% heat-inactivated bovine serum (Gibco)) and filtered through 40 μ m nylon mesh (Sefar). Thymocytes and splenocytes were isolated by crushing the whole thymus or spleen between two microscope slides followed by pipetting and filtering through nylon mesh. The number of viable cells was determined by diluting the cell with Turk Blood Diluting Fluid (Ricca Chemical) and manually counting using haemocytometer under microscope. To identify different T cell fractions in the thymus, total thymocytes were stained with CD4 (GK1.5, PE), CD8a (53-6.7, APC), and DAPI (2 μ g/ml). To identify hematopoietic stem and progenitor cells by flow cytometry, bone marrow and spleen cells were stained with antibodies against c-kit (2B8, APC-eFluor780), Sca-1 (E13-161.7, PE-Cy7), CD48 (HM48-1, APC), CD150 (TC15-12F12.2, PE), as well as biotin-conjugated antibodies against the following lineage markers: CD2 (RM2-5), CD3e (145-2c11), CD4 (GK1.5), CD5 (53-7.3), CD8a (53-6.7), B220 (RA3-6B2); Mac-1 (M1/70), Gr-1 (RB6-8C5), and Ter119 (TER-119), followed by staining with PE-CF594 conjugated streptavidin (BD Biosciences) and DAPI (2 μ g/ml). All antibodies were used 1:200 with all stainings carried out on ice for 30 minutes. All primary and secondary antibodies were purchased from eBiosciences and Biolegend unless otherwise indicated. Flow cytometry analysis of stained cells was performed on a customized LSR II 7-laser, 17-color flow cytometer (Becton-Dickinson), and recorded data was analyzed in BD FACSDiva 8.0.1 and FlowJo 10.0.8 software. For analysis, single cells were gated using FSC-A x FSC-H parameters. Debris was excluded on a FSC-A x SSC-A plot. Live cells (DAPI-) were selected for further analysis. Live total thymocytes were fractionated according to the following cell surface phenotypes: CD4 + T cells: CD4 + CD8-, CD8 + T cells: CD4-CD8 +, double-positive T cells: CD4 + CD8 +, double negative T cells: CD4-CD8-. Hematopoietic stem cells were identified from total live bone marrow cells or splenocytes by first gating out cells positive for the lineage markers (CD2+, CD3+, CD4+, CD5+, CD8+, B220+, Ter119+, Mac-1+, Gr-1 +), followed by gating on the Sca-1+c-kit+ cell population. Lineage-Sca-1+c-kit+ cells were then fractionated according to CD150 and CD48 expression to identify HSCs with the following cell surface phenotype: Lineage-Sca-1+c-kit+CD150 + CD48-.

RNA library preparation and sequencing analysis

Liver was excised from P60 WT, P60 miR-29TG, and 2-year-old mice, and total RNA was isolated using the miRNeasy kit (Qiagen). RNA libraries were prepared using Illumina TruSeq (polyA +) and sequencing was performed on the Illumina HiSeq 2500 platform at the UNC High Through Sequencing Core Facility, yielding an average of ~71 reads across samples. Sequencing reads were mapped to the GENCODE mouse transcriptome (vM10) using STAR (v2.4.2a) and transcripts were quantified using SALMON (v0.6.0). Across the samples, ~80% of the reads were mappable. Transcript counts were normalized and differentially expressed genes (using FDR < 0.1) were identified using DESeq2 (v1.16.1). Raw sequencing data are available through GEO accession ID GSE107763.

miRHub analysis

First, we used the seed-based target prediction algorithm TargetScan5.2⁶³ to determine for each miRNA the number of predicted conserved targets among the genes in our gene sets. Each predicted miRNA-gene interaction was assigned a score based on the strength of the seed match, the level of conservation of the target site, the number of predicted target sites, and the clustering of target sites within that gene's 3' UTR. Finally, for each miRNA, the final targeting score was calculated by summing the scores across all genes and dividing by the number of genes. We repeated this procedure 10,000 times, with a new set of randomly selected mouse genes each time, in order to generate a background distribution of the predicted targeting scores for each miRNA (genes and corresponding 3' UTR sequences were downloaded from <http://www.targetscan.org>).

These score distributions were then used to calculate an empirical p-value of the targeting score for each miRNA in our gene set. To account for differences in the average 3' UTR length between the genes of interest and the randomly selected genes in each simulation, the targeting score was normalized by 3' UTR length.

Pathway enriched analysis

Significantly differentially expressed genes (DEG) were defined as those with FDR < 0.1. Up- and downregulated DEG lists were analyzed for enrichment in biological pathways using the online tool Enrichr⁶⁴, which shows results from all available pathway databases. All pathway enrichment results shown in this manuscript are from the use of the Enrichr tool.

Statistics and reproducibility

Statistical analyses were performed using GraphPad Prism 9 software. Data are expressed as mean ± s.e.m. in bar plots or median, minimum, and maximum in box and whiskers plots. Measurements were taken from distinct samples. The Student's *t*-test (unpaired, two-tailed) for parametric data was used for the analysis of two groups unless stated otherwise. No statistical methods were used to predetermine sample sizes, but our sample sizes are consistent with those reported in previous publications.

Reporting summary

Further information on research design is available in the Nature Portfolio Reporting Summary linked to this article.

Data availability

The data underlying the results in Fig. 4 are provided in Supplementary Data 1 and 2. The source data used to generate the graphs in this manuscript are compiled in Supplementary Data 4. The miR-29-expressing ES clones used to generate the miR-29TG mice are available at the NCI Mouse Repository (ES Cell Lines Catalog: M000108). The sequencing data reported in this paper have been deposited in Gene Expression Omnibus (GEO): GSE107763. Further information and requests for resources and reagents should be directed to corresponding author, Mohanish Deshmukh (mohanish@med.unc.edu).

Received: 27 February 2023; Accepted: 14 August 2024;

Published online: 27 August 2024

References

- Bartel, D. P. Metazoan MicroRNAs. *Cell* **173**, 20–51 (2018).
- Diener, C., Keller, A. & Meese, E. Emerging concepts of miRNA therapeutics: from cells to clinic. *Trends Genet.* **38**, 613–626 (2022).
- Rupaimoole, R. & Slack, F. J. MicroRNA therapeutics: towards a new era for the management of cancer and other diseases. *Nat. Rev. Drug Discov.* **16**, 203–222 (2017).
- Kole, A. J., Swahari, V., Hammond, S. M. & Deshmukh, M. miR-29b is activated during neuronal maturation and targets BH3-only genes to restrict apoptosis. *Genes Dev.* **25**, 125–130 (2011).
- Dalgaard, L. T., Sørensen, A. E., Hardikar, A. A. & Joglekar, M. V. The microRNA-29 family: role in metabolism and metabolic disease. *Am. J. Physiol. Cell Physiol.* **323**, C367–c377 (2022).
- Hung, Y. H. et al. MiR-29 regulates de novo lipogenesis in the liver and circulating triglyceride levels in a Sirt1-dependent manner. *Front. Physiol.* **10**, 1367 (2019).
- Kurtz, C. L. et al. Inhibition of miR-29 has a significant lipid-lowering benefit through suppression of lipogenic programs in liver. *Sci. Rep.* **5**, 12911 (2015).
- O'Connor, S. et al. AGO HITS-CLIP reveals distinct miRNA regulation of white and brown adipose tissue identity. *Genes Dev.* **35**, 771–781 (2021).
- Hung, Y. H. et al. Acute suppression of insulin resistance-associated hepatic miR-29 in vivo improves glycemic control in adult mice. *Physiol. Genomics* **51**, 379–389 (2019).
- Swahari, V. et al. MicroRNA-29 is an essential regulator of brain maturation through regulation of CH methylation. *Cell Rep.* **35**, 108946 (2021).
- Napoli, D. et al. MiR-29 coordinates age-dependent plasticity brakes in the adult visual cortex. *EMBO Rep.* **21**, e50431 (2020).
- Ma, F. et al. The microRNA miR-29 controls innate and adaptive immune responses to intracellular bacterial infection by targeting interferon- γ . *Nat. Immunol.* **12**, 861–869 (2011).
- Yee Mon, K. J. et al. MicroRNA-29 specifies age-related differences in the CD8+ T cell immune response. *Cell Rep.* **37**, 109969 (2021).
- Jiang, H., Zhang, G., Wu, J. H. & Jiang, C. P. Diverse roles of miR-29 in cancer. *Oncol. Rep.* **31**, 1509–1516 (2014).
- van Rooij, E. et al. Dysregulation of microRNAs after myocardial infarction reveals a role of miR-29 in cardiac fibrosis. *Proc. Natl Acad. Sci. USA* **105**, 13027–13032 (2008).
- Somel, M. et al. MicroRNA, mRNA, and protein expression link development and aging in human and macaque brain. *Genome Res.* **20**, 1207–1218 (2010).
- Dimmeler, S. & Nicotera, P. MicroRNAs in age-related diseases. *EMBO Mol. Med.* **5**, 180–190 (2013).
- Caravia, X. M. & López-Otín, C. Regulatory roles of miRNAs in aging. *Adv. Exp. Med. Biol.* **887**, 213–230 (2015).
- Wagner, V. et al. Characterizing expression changes in noncoding RNAs during aging and heterochronic parabiosis across mouse tissues. *Nat. Biotechnol.* **42**, 109–118 (2024).
- Kozomara, A., Birgaoanu, M. & Griffiths-Jones, S. miRBase: from microRNA sequences to function. *Nucleic Acids Res.* **47**, D155–d162 (2019).
- Zhou, Y. et al. A secreted microRNA disrupts autophagy in distinct tissues of *Caenorhabditis elegans* upon ageing. *Nat. Commun.* **10**, 4827 (2019).
- Ugalde, A. P. et al. Aging and chronic DNA damage response activate a regulatory pathway involving miR-29 and p53. *EMBO J.* **30**, 2219–2232 (2011).
- Takahashi, M., Eda, A., Fukushima, T. & Hohjoh, H. Reduction of type IV collagen by upregulated miR-29 in normal elderly mouse and *klotho*-deficient, senescence-model mouse. *PLoS ONE* **7**, e48974 (2012).
- Caravia, X. M., Roiz-Valle, D., Morán-Álvarez, A. & López-Otín, C. Functional relevance of Functional miRNAs in premature aging. *Mech. Ageing Dev.* **168**, 10–19 (2017).
- Bates, D. J. et al. MicroRNA regulation in Ames dwarf mouse liver may contribute to delayed aging. *Aging Cell* **9**, 1–18 (2010).
- Osorio, F. G. et al. Splicing-directed therapy in a new mouse model of human accelerated aging. *Sci. Transl. Med.* **3**, 106ra107 (2011).
- Kriegel, A. J., Liu, Y., Fang, Y., Ding, X. & Liang, M. The miR-29 family: genomics, cell biology, and relevance to renal and cardiovascular injury. *Physiol. Genomics* **44**, 237–244 (2012).
- Bergo, M. O. et al. *Zmpste24* deficiency in mice causes spontaneous bone fractures, muscle weakness, and a prelamins A processing defect. *Proc. Natl Acad. Sci. USA* **99**, 13049–13054 (2002).
- Pendas, A. M. et al. Defective prelamins A processing and muscular and adipocyte alterations in *Zmpste24* metalloproteinase-deficient mice. *Nat. Genet.* **31**, 94–99 (2002).
- Caravia, X. M. et al. The microRNA-29/PGC1 α regulatory axis is critical for metabolic control of cardiac function. *PLoS Biol.* **16**, e2006247 (2018).
- Smith, K. M. et al. miR-29ab1 deficiency identifies a negative feedback loop controlling Th1 bias that is dysregulated in multiple sclerosis. *J. Immunol.* **189**, 1567–1576 (2012).

32. López-Otín, C., Blasco, M. A., Partridge, L., Serrano, M. & Kroemer, G. Hallmarks of aging: an expanding universe. *Cell* **186**, 243–278 (2023).
33. Imai, S. & Guarente, L. NAD⁺ and sirtuins in aging and disease. *Trends Cell Biol.* **24**, 464–471 (2014).
34. Chen, Y. et al. Cyclic stretch and compression forces alter microRNA-29 expression of human periodontal ligament cells. *Gene* **566**, 13–17 (2015).
35. Lago, J. C. & Puzzi, M. B. The effect of aging in primary human dermal fibroblasts. *PLoS ONE* **14**, e0219165 (2019).
36. Loerch, P. M. et al. Evolution of the aging brain transcriptome and synaptic regulation. *PLoS ONE* **3**, e3329 (2008).
37. Wang, R. et al. B7-H3 suppresses doxorubicin-induced senescence-like growth arrest in colorectal cancer through the AKT/TM4SF1/SIRT1 pathway. *Cell Death Dis.* **12**, 453 (2021).
38. Wei, Q. et al. JAZF1 ameliorates age and diet-associated hepatic steatosis through SREBP-1c-dependent mechanism. *Cell Death Dis.* **9**, 859 (2018).
39. Koonen, D. P. Y. et al. CD36 expression contributes to age-induced cardiomyopathy in mice. *Circulation* **116**, 2139–2147 (2007).
40. Chong, M. et al. CD36 initiates the secretory phenotype during the establishment of cellular senescence. *EMBO Rep.* **19**, e45274 (2018).
41. Saitou, M. et al. An evolutionary transcriptomics approach links CD36 to membrane remodeling in replicative senescence. *Mol. Omics* **14**, 237–246 (2018).
42. Hu, Z. et al. MicroRNA-29 induces cellular senescence in aging muscle through multiple signaling pathways. *Aging* **6**, 160–175 (2014).
43. Bartel, D. P. MicroRNAs: genomics, biogenesis, mechanism, and function. *Cell* **116**, 281–297 (2004).
44. Baumgart, M. et al. Age-dependent regulation of tumor-related microRNAs in the brain of the annual fish *Nothobranchius furzeri*. *Mech. Ageing Dev.* **133**, 226–233 (2012).
45. Kudlow, B. A., Kennedy, B. K. & Monnat, R. J. Werner and Hutchinson-Gilford progeria syndromes: mechanistic basis of human progeroid diseases. *Nat. Rev. Mol. Cell Biol.* **8**, 394–404 (2007).
46. Zhang, X. et al. CaMKIV-dependent preservation of mtor expression is required for autophagy during lipopolysaccharide-induced inflammation and acute kidney injury. *J. Immunol.* **193**, 2405–2415 (2014).
47. Dzakah, E. E. et al. Loss of miR-83 extends lifespan and affects target gene expression in an age-dependent manner in *Caenorhabditis elegans*. *J. Genet. Genomics* **45**, 651–662 (2018).
48. Neves, J. & Sousa-Victor, P. Regulation of inflammation as an anti-aging intervention. *FEBS J.* **287**, 43–52 (2020).
49. Ferrucci, L. & Fabbri, E. Inflammageing: chronic inflammation in ageing, cardiovascular disease, and frailty. *Nat. Rev. Cardiol.* **15**, 505–522 (2018).
50. Zheng, R. et al. The complement system, aging, and aging-related diseases. *Int. J. Mol. Sci.* **23**, 8689 (2022).
51. Kurtz, C. L. et al. MicroRNA-29 fine-tunes the expression of key FOXA2-activated lipid metabolism genes and is dysregulated in animal models of insulin resistance and diabetes. *Diabetes* **63**, 3141–3148 (2014).
52. Whitton, H. et al. Changes at the nuclear lamina alter binding of pioneer factor Foxa2 in aged liver. *Aging Cell* **17**, e12742 (2018).
53. Sassi, Y. et al. Cardiac myocyte miR-29 promotes pathological remodeling of the heart by activating Wnt signaling. *Nat. Commun.* **8**, 1614 (2017).
54. Wei, W. et al. miR-29 targets Akt3 to reduce proliferation and facilitate differentiation of myoblasts in skeletal muscle development. *Cell Death Dis.* **4**, e668–e668 (2013).
55. Rusu-Nastase, E. G. et al. MiR-29a increase in aging may function as a compensatory mechanism against cardiac fibrosis through SERPINH1 downregulation. *Front Cardiovasc Med* **8**, 810241 (2021).
56. Horita, M., Farquharson, C. & Stephen, L. A. The role of miR-29 family in disease. *J. Cell. Biochem.* **122**, 696–715 (2021).
57. Pereira, P. A., Tomas, J. F., Queiroz, J. A., Figueiras, A. R. & Sousa, F. Recombinant pre-miR-29b for Alzheimer’s disease therapeutics. *Sci. Rep.* **6**, 19946 (2016).
58. Liu, M. N., Luo, G., Gao, W. J., Yang, S. J. & Zhou, H. miR-29 family: a potential therapeutic target for cardiovascular disease. *Pharmacol. Res.* **166**, 105510 (2021).
59. Carrero, D., Soria-Valles, C. & López-Otín, C. Hallmarks of progeroid syndromes: lessons from mice and reprogrammed cells. *Dis. Model Mech.* **9**, 719–735 (2016).
60. Prosser, H. M., Koike-Yusa, H., Cooper, J. D., Law, F. C. & Bradley, A. A resource of vectors and ES cells for targeted deletion of microRNAs in mice. *Nat. Biotechnol.* **29**, 840 (2011).
61. Bouxsein, M. L. et al. Guidelines for assessment of bone microstructure in rodents using micro-computed tomography. *J. Bone Miner. Res.* **25**, 1468–1486 (2010).
62. He, S. et al. Transient CDK4/6 inhibition protects hematopoietic stem cells from chemotherapy-induced exhaustion. *Sci. Transl. Med.* **9**, eaal3986 (2017).
63. Grimson, A. et al. MicroRNA targeting specificity in mammals: determinants beyond seed pairing. *Mol. Cell* **27**, 91–105 (2007).
64. Kuleshov, M. V. et al. Enrichr: a comprehensive gene set enrichment analysis web server 2016 update. *Nucleic Acid Res.* **44**, W90–W97 (2016).

Acknowledgements

The authors thank Dr. Peter J Havel (UC Davis) for sharing monkey tissue samples. We also thank Dr. Greg Hannon for sending us the mouse embryonic stem cells overexpressing miR-29b that we used to generate the miR-29TG mice. We appreciate the help of Mervi Eeva, Ying Li, and Bentley Midkiff at the UNC Translational Pathology Laboratory (TPL) for expert technical assistance and Dr. Dale Cowley for assistance in generating the miR-29 transgenic mice. We also thank Janice Weaver and Carolyn Suitt at the UNC Animal Histopathology and the Center for Gastrointestinal Biology and Disease (CGIBD), respectively, as well as Dr. Andrew Troy for assistance in isolating muscle tissue. The UNC TPL is supported in part by grants from the National Cancer Institute (P30CA016080) and the UNC University Cancer Research Fund. We thank the Small Animal Imaging Facility at the UNC Biomedical Imaging Research Center for providing the microCT imaging service. This work was supported by grants from the European Union (ERC-Advanced Grant, 742067), Ministerio de Ciencia e Innovación (Spain) (SAF2017-87655-R, PDI2020-118394RB-I00), American Diabetes Association Pathway award 1-16-ACE-47 to P.S., and NIH grants R01DK105965 to P.S. and NIH grants AG082140 and AG055304 to M.D.; X.M.C. was supported by FPU fellowship (Ministerio de Educación, Spain).

Author contributions

A.N. and V.S. conducted most of the experiments with help as described here. Y-H.H, M.K., C.L.K., J.B.G., and P.S. assisted in analyzing the RNAseq data. E.H., S.H., J.K., V.P., C.F., M.B., S.K., and N.S. assisted in conducting experiments that characterized the miR-29TG mice. X.M.C., D.R.V., and C.L.O. generated the miR-29-deficient mice and conducted the experiments involving the *Lmna*^{6609G} and *Zmpste24*^{-/-} miR-29-deficient mice. A.N., V.S., and M.D. outlined the project. M.D. and P.S. supervised the project, and E.H., A.N., V.S., P.S., and M.D. produced the final version of the manuscript.

Competing interests

The authors declare no competing interests.

Ethical approval

All animal handling and experiments were approved and conducted in accordance with local Animal Experimental Ethics Committees. We have complied with all relevant ethical regulations for animal use.

Additional information

Supplementary information The online version contains supplementary material available at <https://doi.org/10.1038/s42003-024-06735-z>.

Correspondence and requests for materials should be addressed to Praveen Sethupathy or Mohanish Deshmukh.

Peer review information *Communications Biology* thanks Ilya Vinnikov, Frank Slack and the other, anonymous, reviewer(s) for their contribution to the peer review of this work. Primary Handling Editors: Gracjan Michlewski, Anam Akhtar and Kaliya Georgieva.

Reprints and permissions information is available at <http://www.nature.com/reprints>

Publisher's note Springer Nature remains neutral with regard to jurisdictional claims in published maps and institutional affiliations.

Open Access This article is licensed under a Creative Commons Attribution-NonCommercial-NoDerivatives 4.0 International License, which permits any non-commercial use, sharing, distribution and reproduction in any medium or format, as long as you give appropriate credit to the original author(s) and the source, provide a link to the Creative Commons licence, and indicate if you modified the licensed material. You do not have permission under this licence to share adapted material derived from this article or parts of it. The images or other third party material in this article are included in the article's Creative Commons licence, unless indicated otherwise in a credit line to the material. If material is not included in the article's Creative Commons licence and your intended use is not permitted by statutory regulation or exceeds the permitted use, you will need to obtain permission directly from the copyright holder. To view a copy of this licence, visit <http://creativecommons.org/licenses/by-nc-nd/4.0/>.

© The Author(s) 2024